American Mineralogist, Volume 80, pages 897–906, 1995

Structural modulation and phase transition in a Na-rich alkali feldspar

Huifang Xu,* David R. Veblen
Department of Earth and Planetary Sciences, Johns Hopkins University, Baltimore, Maryland 21218, U.S.A.
Yiqiang Zhang
Department of Earth and Planetary Sciences, Johns Hopkins University, Baltimore, Maryland 21218, U.S.A.; and S. S. Papadopulos & Associates, Inc., 7944 Wisconsin Avenue, Bethesda, Maryland 20814, U.S.A.

Abstract

Transmission electron microscopy (TEM) revealed a commensurate modulated structure in a Na-rich alkali feldspar ($Ab_{66}Or_{29}An_5$) from a basalt from Anhui Province, China. High-resolution TEM images with wavelike (001) lattice fringes directly reveal one-dimensional modulation waves in the crystal. The average modulation period along the **b** axis is $14d_{010}$ ($\cong$180 Å), although both larger and smaller spacings have been observed. The modulated structure can be described as periodic stacking of (010) layer domains following the albite twin law. The relationship between the extended cell (supercell) of the modulated structure and the normal alkali feldspar unit cell (subcell) is as follows: $\mathbf{a}_{sup} \cong \mathbf{a}_{sub}$, $\mathbf{b}_{sup} \cong 14\mathbf{b}_{sub}$, $\mathbf{c}_{sup} \cong \mathbf{c}_{sub}$, $\beta_{sup} \cong \beta_{sub}$ (subscripts "sup" and "sub" indicate the supercell and subcell, respectively). A possible space group for the modulated structure is *Pm*.

In situ heating and cooling experiments suggest that the phase transition in this feldspar thin foil might be a weakly first-order and displacive transformation. The transition temperature is close to 500 °C for the crystal examined. The modulated structure formed during the phase transition of the feldspar from $C2/m$ symmetry to $C\bar{1}$ at a rapid cooling rate.

A heuristic nonlinear dynamics model for the arrangement of triclinic domains in the feldspar at the phase transition from monoclinic to triclinic symmetry was developed on the basis of a Landau potential, a damping term accounting for the structural differences among neighboring units, and a periodic force in the crystal along the **b** axis. Numerical solutions indicate that periodic modulation arises during the monoclinic to triclinic transition only under special conditions relatively far from equilibrium, and a nonperiodic arrangement of triclinic domains along the **b** axis is the more general case. Therefore, according to this model, the modulated structure is a metastable and intermediate structure between monoclinic ($C2/m$) and triclinic ($C\bar{1}$) phases. This type of modulated structure in Na-rich alkali feldspars may indicate high-temperature growth as a monoclinic crystal, followed by very rapid cooling into the triclinic stability field.

Introduction

Some Na-rich alkali feldspars are triclinic (i.e., anorthoclase) and commonly show cross-hatched twinning (Deer et al., 1965; Winchell and Winchell, 1967; Smith and Brown, 1988). Some Na-rich alkali feldspar crystals, however, appear to be monoclinic (i.e., sodian sanidine) (Smith and Brown, 1988). As a further complication, McConnell (1971) and Owen and McConnell (1974) found a very fine-scale exsolution texture in some sodian sanidine crystals. They interpreted the exsolution texture as resulting from coherent spinodal decomposition. The exsolved Ab-rich and Or-rich phases were intergrown nearly parallel to $(\bar{6}01)$, and both were monoclinic (Ab = $NaAlSi_3O_8$, Or = $KAlSi_3O_8$).

Two structurally distinct mechanisms induce phase transitions from monoclinic ($C2/m$) to triclinic ($C\bar{1}$) symmetry in Ab-rich alkali feldspars. One is displacement-induced collapse of the aluminosilicate framework (e.g., the monalbite to analbite transition), and the other is Al-Si order-induced breaking of the monoclinic symmetry (e.g., the monalbite to albite transition) (Kroll et al., 1980). The displacive transition temperatures for Ab-rich alkali feldspars vary almost linearly with respect to their Or content (Kroll et al., 1980). In general, the anorthite component (An = $CaAl_2Si_2O_8$) in alkali feldspars increases the displacive phase-transition temperature (Kroll and Bambauer, 1971). During the transition from monoclinic to triclinic symmetry, feldspars generally develop relatively fine-scale albite twins (Ribbe, 1983; Laves, 1950, 1960). If the triclinic domains are arranged periodically in the albite-twin relationship, a modulated structure results in alkali feldspar (Ribbe, 1983).

* Present address: Department of Geology, Arizona State University, Tempe, Arizona 85287, U.S.A.

0003–004X/95/0910–0897$02.00

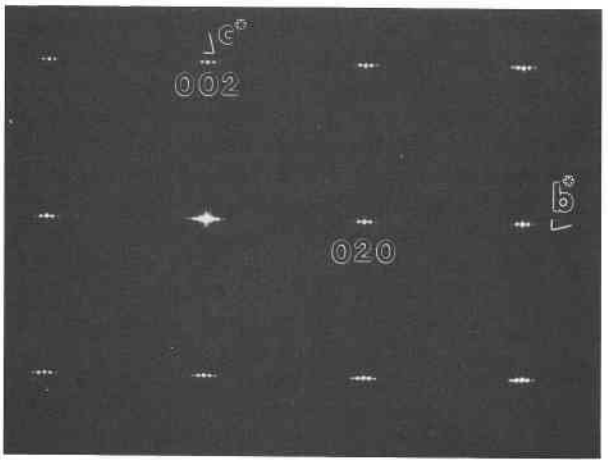

Fig. 1. A [100] zone-axis electron diffraction pattern of the Na-rich feldspar from Nusan Hill, Anhui Province, China, showing main Bragg reflections flanked by satellite reflections.

Most natural, high-temperature, Na-rich alkali feldspars with appreciable anorthite component crystallized at relatively high temperatures, and they typically exsolved by coherent spinodal decomposition, underwent a displacive phase transition from $C2/m$ to $C\bar{1}$ symmetry, or both. Previous transmission electron microscopy (TEM) studies of exsolution textures in sodian sanidine were described by Owen and McConnell (1974), and TEM investigation of cross-hatched transformation twinning in triclinic anorthoclase was described by Smith et al. (1987). In this paper, we describe a periodic, modulated structure with monoclinic symmetry in a natural Na-rich feldspar quenched from high temperature. The modulated structure formed during a displacive phase transition. We also introduce a nonlinear dynamics model that reproduces the periodic modulation. A preliminary report of this work was presented by Xu and Veblen (1993) in the NATO Advanced Study Institute on Feldspars and Their Reactions.

Sample description and experimental techniques

The Na-rich alkali feldspar megacryst for this TEM study was obtained from a Cenozoic alkali-olivine basalt at Nusan Hill, Anhui Province, China. The crystal is glassy and transparent. Other inclusions in the basalt are corundum, Al-rich augite, and pyrope megacrysts, as well as lherzolite nodules. All the large crystals were crystallized in basaltic magma at high pressure and temperature (Zhou and Chen, 1982). Crystals quenched from high temperature generally have a disordered Al-Si distribution. The feldspar crystal exhibits monoclinic optics, with an optic angle ($2V$) of 55°. The X-ray powder diffraction pattern shows very broad 131 diffraction peaks. It can be inferred that the unit-cell scale of triclinic domains in the feldspar may account for the 131 peak broadening.

Thin specimens were prepared for the TEM and in situ heating studies by Ar ion milling and then coated with a thin layer of C. All TEM and analytical electron microscopy (AEM) investigations were performed with a Philips EM420ST transmission electron microscope operated at 120 keV and equipped with an EDAX energy-dispersive X-ray detector and a Princeton Gamma Tech analyzer. The average chemical composition of the feldspar is $Ab_{66}Or_{29}An_5$, as determined by both AEM and electron microprobe analysis using mineral standards. The in situ heating experiments were performed with a single-tilt Gatan heating specimen holder. The average heating and cooling rates were about 20 °C/min and were monitored with a thermocouple embedded in the heater block.

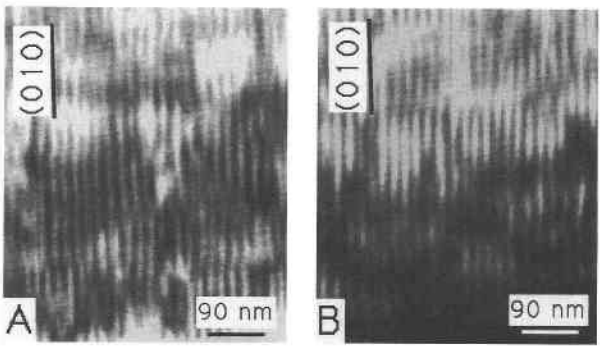

Fig. 2. Bright-field (BF) image (**A**) and dark-field (DF) (**g** = 001) image (**B**) of the Na-rich feldspar, showing one-dimensional modulation along the **b** axis and irregularities in modulation periodicity.

TEM results and interpretation

Electron diffraction and TEM images

Selected-area electron diffraction (SAED) patterns obtained with the electron beam parallel to the feldspar [100] zone axis show main Bragg reflections with satellite reflections and weak streaking along **b*** (Fig. 1). The satellites indicate that there is a one-dimensional modulated structure in the crystal, and their spacing shows that the modulation period is $14d_{010}$ (≅180 Å) and thus is commensurate (i.e., there is an integral number of subcells in the supercell). Bright-field (BF) and dark-field (DF) images (Fig. 2A and 2B) also show the modulation with an average period of 180 Å along the **b** axis. In addition, the images show irregularities of the modulation period and out-of-phase boundaries like those described by Veblen (1985) in localized areas, which produce the weak streaking in SAED patterns. In some areas of the crystal, the [100] zone-axis SAED pattern shows very weak satellite reflections along **c***, in addition to those along **b***. A [$\bar{1}$01] zone-axis electron diffraction pattern (Fig. 3A) and its corresponding DF image (**g** = 111; Fig. 3B) show satellite reflections and the same modulation as in Figure 2. The satellite reflections (e.g., those near the 131 reflection) may be responsible for some of the pronounced broadening observed in X-ray powder diffraction peaks. However, a sodian sanidine crystal ($Ab_{57}Or_{39}An_4$) from another Cenozoic alkali basalt of Shen County, Zhejiang Province, with a weak tweed texture (two-dimensional

modulations with an average modulation period of 100 Å along the **b** and **c** directions), produces a relatively sharp 131 X-ray diffraction peak (Xu, 1993).

In the DF image of Figure 3B, there is also very weak contrast with a relatively long period normal to **b*** (i.e., horizontal in the figure). This kind of contrast is probably caused by weak compositional modulations involving separation of Na and K because of spinodal decomposition of the crystal. However, with AEM we were unable to demonstrate compositional differences in these areas of weak contrast within experimental error. Therefore, if the crystal had begun to undergo exsolution, the incipient compositional differences remain quite small.

HRTEM images and structural model

A high-resolution transmission electron microscopic (HRTEM) image of the feldspar sample corresponding to the orientation of Figure 1 shows straight (010) lattice fringes and wavelike (001) fringes (Fig. 4). If the specimen is tilted slightly around **c***, its HRTEM image shows only the wavelike (001) lattice fringes. Measurements from the HRTEM images show that this modulation wave has an average period of approximately 180 Å, or $14d_{010}$, within measurement error. The modulated structure can be thought of as periodic stacking of triclinic (010) layer domains in the albite-twin relationship. The boundary positions between neighboring (010) layer domains are the positions of mirror planes in the modulated structure. Figure 5 illustrates a schematic structural model for the modulated feldspar with sinusoidal (001) lattice planes and straight (010) planes. The relationship between the extended cell (supercell) of the modulated structure and the usual monoclinic alkali feldspar subcell is as follows: $\mathbf{a}_{sup} \cong \mathbf{a}_{sub}$, $\mathbf{b}_{sup} \cong 14\mathbf{b}_{sub}$, $\mathbf{c}_{sup} \cong \mathbf{c}_{sub}$, $\beta_{sup} \cong \beta_{sub}$ (subscripts "sup" and "sub" refer to supercell and subcell, respectively). A possible space group for the supercell of the modulated structure is *Pm*. A similar modulated structure was found in an orthoclase (Xu et al., 1995).

HRTEM images from areas containing the weak modulation along **c*** show wavelike (010) lattice fringes (Fig. 6). Layer domains in this area are also triclinic. The neighboring triclinic layer domains in this area are related by twofold rotation axes parallel to the **b** axis. From this geometry, we conclude that these triclinic layer domains are in the pericline-twin relationship. Such a local modulation causes weak satellite reflections along **c*** in the [100] zone SAED pattern (Fig. 1). Figure 7 illustrates schematically the structural relationship between neighboring triclinic layer domains for this kind of modulation. Relatively higher strain energy in the domain boundaries probably explains the less common occurrence of such modulation.

In situ heating experiments and formation of the modulated structure

To explore further the modulated structure of the Na-rich feldspar, we performed in situ heating experiments while observing the specimen in the TEM. During heating of the original crystal with modulated structure, there was no obvious change in the bright-field image when the temperature of the furnace holding the specimen was below 535 °C (Figs. 8A, 8B, and 9A). As the temperature of the furnace increased to 535 °C, the intensity of the satellite reflections decreased dramatically (Fig. 8C), and only first-order satellite reflections were observed in the diffraction pattern as opposed to the second- and third-order satellites commonly recorded at lower temperatures. The crystal at this temperature showed a weaker and less regular modulation (Fig. 9B). It was also ob-

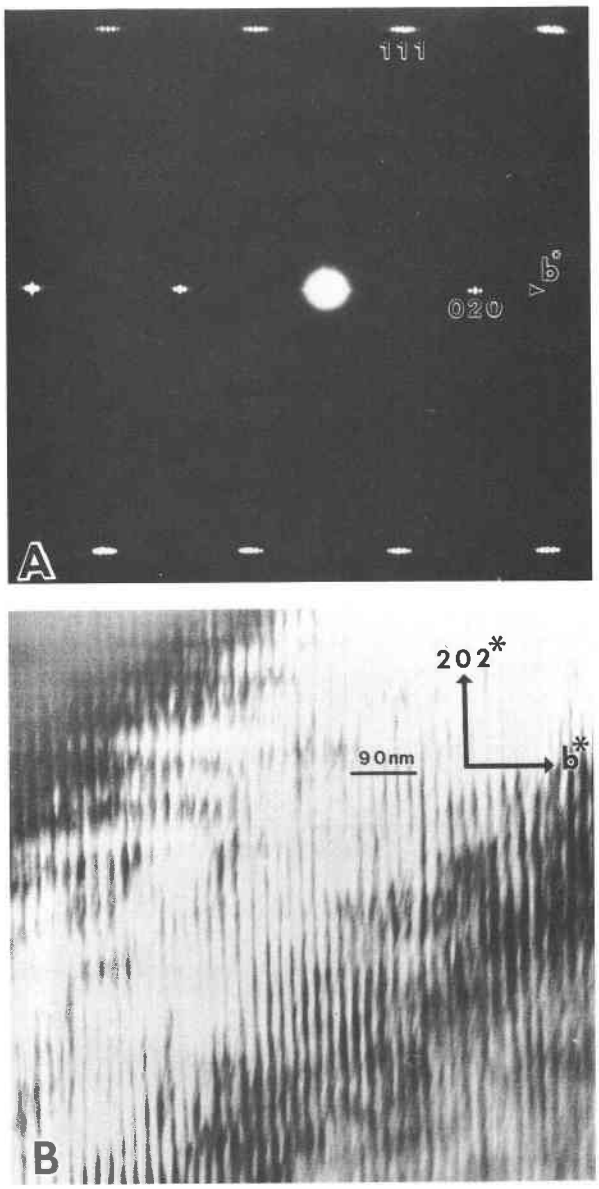

Fig. 3. (**A**) A [$\bar{1}$01] zone-axis SAED pattern showing main Bragg reflections and satellite reflections along **b***. (**B**) A DF image (**g** = 111) of the Na-rich feldspar crystal in the same orientation as **A**, showing one-dimensional modulation along the **b** axis.

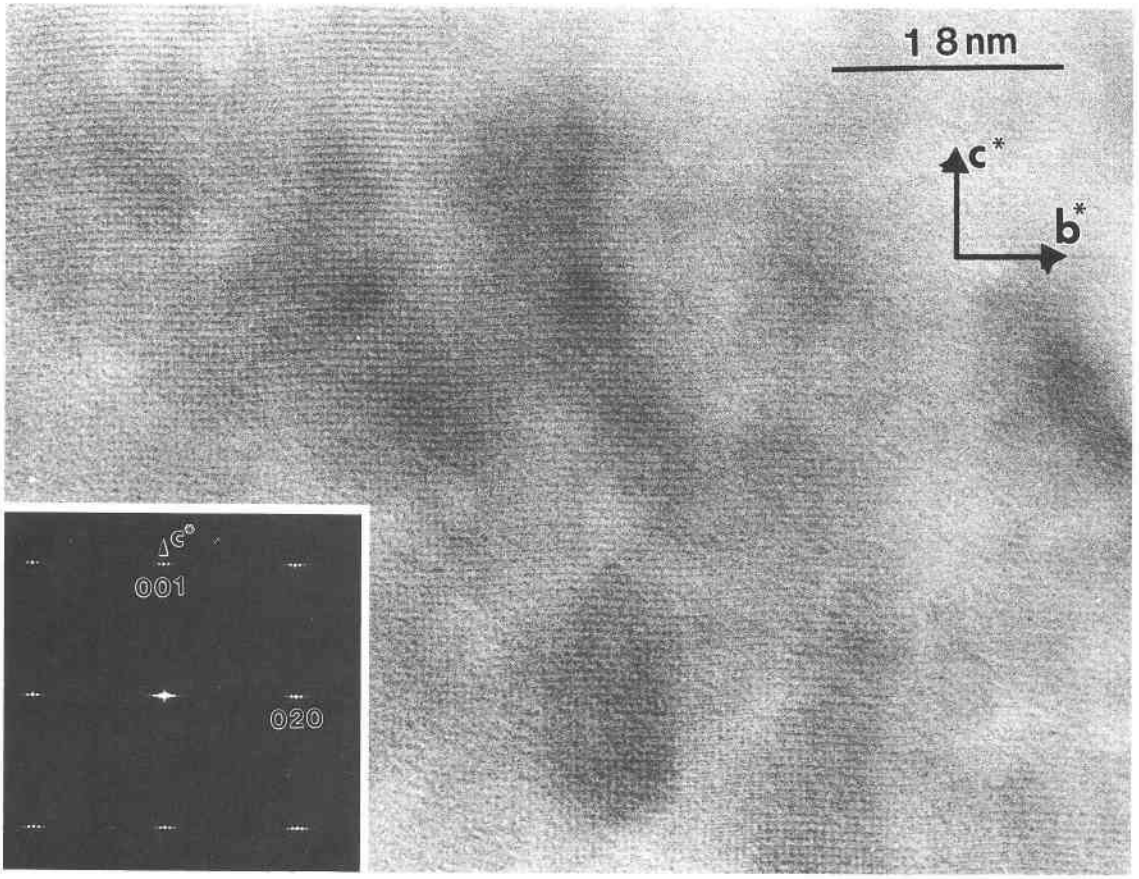

Fig. 4. HRTEM image of the modulated Na-rich feldspar normal to the **a** axis, showing wavelike (001) lattice fringes and straight (010) lattice fringes. The modulation period is $14d_{010}$ (i.e., about 180 Å).

served that the superlattice fringes characteristic of the structural modulation appeared to be vibrating, which hints at a displacive character for the modulation. Further heating of the specimen above 535 °C resulted in further decreases in the intensity of satellite reflections

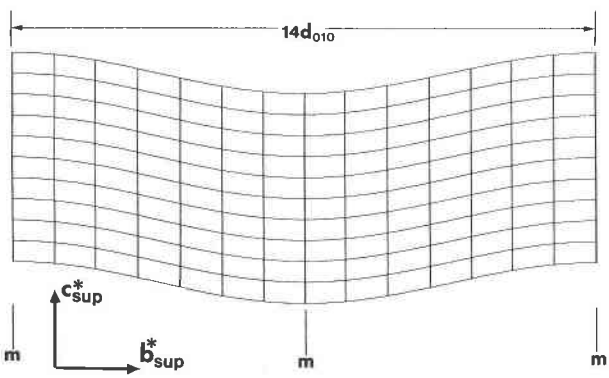

Fig. 5. A schematic structural model of the modulated Na-rich feldspar, showing wavelike (001) lattice planes and straight (010) lattice planes. Each small block represents a triclinic feldspar subcell. Neighboring triclinic domains are in the albite-twin relationship.

(Fig. 8D), but the average modulation period remained almost constant. As the temperature was raised to 702 °C, the satellite reflections were no longer observable (Fig. 8E), and no structural modulation was visible in images (Fig. 9C), except some contrast anomalies owing to out-of-phase boundaries in the original modulated crystal. Further increases in the temperature of the specimen only resulted in further homogenization of the specimen's appearance in the BF image (Fig. 9D).

After reaching 840 °C, the specimen was cooled, and further changes in the SAED pattern and image were recorded. Within the temperature range from 840 to 440 °C, there were no obvious changes. At 440 °C, a weak (010) modulation appeared at the edges of the specimen (Fig. 9E). Its corresponding SAED pattern shows very weak streaking along the **b*** direction but no satellites. The streaking persisted to a temperature of 300 °C, at which satellite reflections with weak streaking reappeared (Fig. 8F). The corresponding image showed obvious modulation (Fig. 9F), although the period of the modulated structure was not as regular as that of the original structure. There are only weak first-order satellite reflections in the diffraction pattern. The average modulation period from measurement of the satellite reflections is

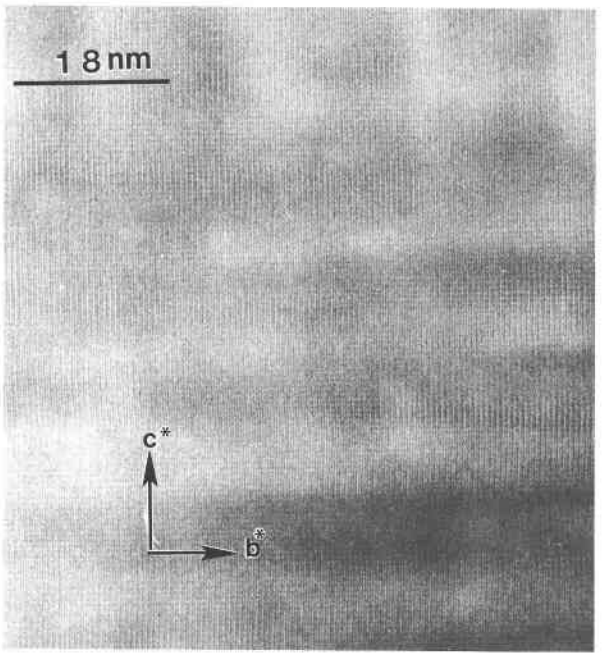

Fig. 6. HRTEM image of the Na-rich feldspar from an area with a weak modulation along **c***, showing wavelike (010) lattice fringes. Best viewed at a low angle parallel to the fringes. Such areas produce SAED patterns with very weak satellite reflections along **c***.

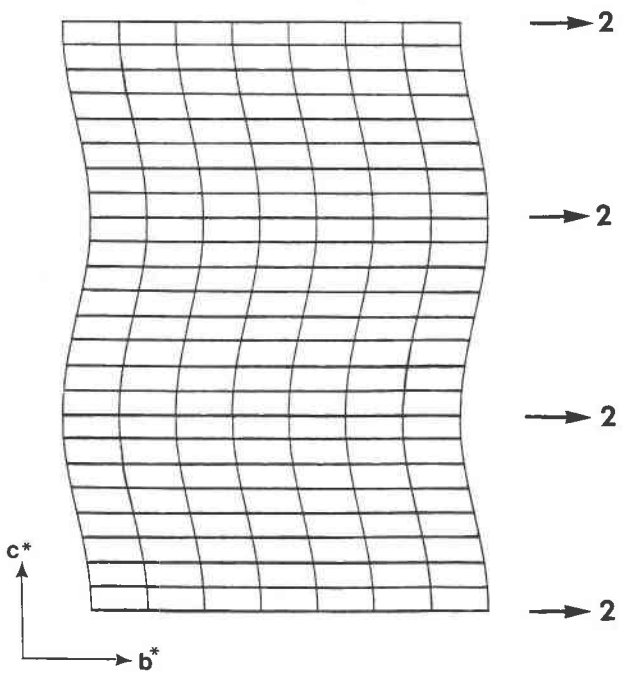

Fig. 7. A schematic structural model of the area with weak modulation along **c*** in Fig. 6. The two neighboring triclinic layer domains are in the pericline-twin relationship (i.e., they are related by twofold rotation axes parallel to the **b** axes of the local lattice).

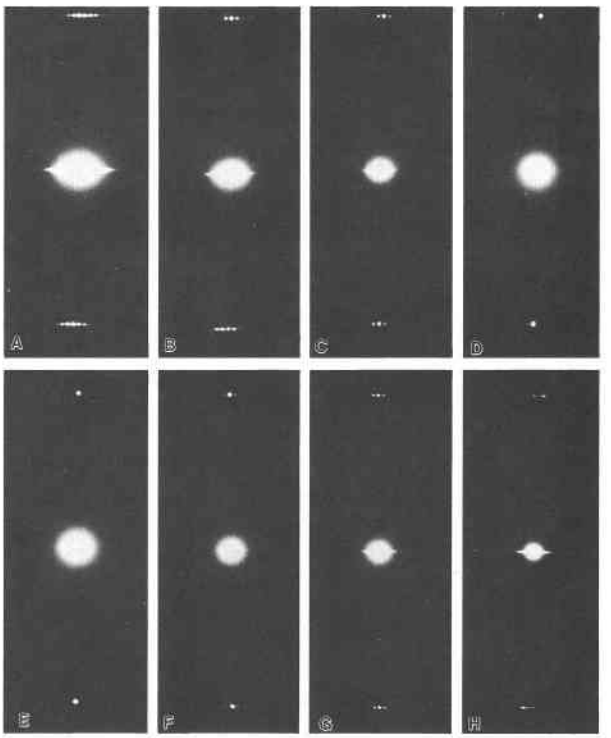

Fig. 8. The 001, 000, and 00$\bar{1}$ reflections from SAED patterns of Na-rich feldspar during heating and cooling. (**A**) 137 °C (heating), (**B**) 366 °C (heating), (**C**) 535 °C (heating), (**D**) 685 °C (heating), (**E**) 702 °C (heating), (**F**) 300 °C (cooling), (**G**) 186 °C (cooling), and (**H**) 25 °C (cooling).

about $16d_{010}$ ($\cong$206 Å). Upon further cooling of the specimen, the intensities of the satellite reflections increased (Fig. 8G). Below 180 °C, however, the modulation periodicity and symmetrical distribution of satellite reflections were gradually lost as the temperature was lowered (Fig. 8H). Between 180 °C and room temperature, the specimen image was characterized by coarser and nonperiodic triclinic (010) layer domains in the albite-twin relationship (Fig. 9G and 9H). HRTEM images of the cooled specimen show nonperiodic albite-twin domains characterized by chevronlike (001) lattice fringes (Fig. 10) rather than the sinusoidal structure of the original specimen.

Two critical temperature values, 535 and 440 °C, characterize the observed structural changes in the Na-rich feldspar sample during heating and cooling, respectively. The phase-transition temperature presumably lies between these two values. After the specimen was cooled and reheated, it showed displacive transitions similar to those of the first heating cycle except for the appearance of periodic modulation during heating, but the transition temperatures were 520 and 482 °C on heating and cooling, respectively. The heat treatment resulted in some permanent structural changes in the crystal. The hysteresis indicated by the differences in the heating and cooling critical temperatures shows that the phase transition is a

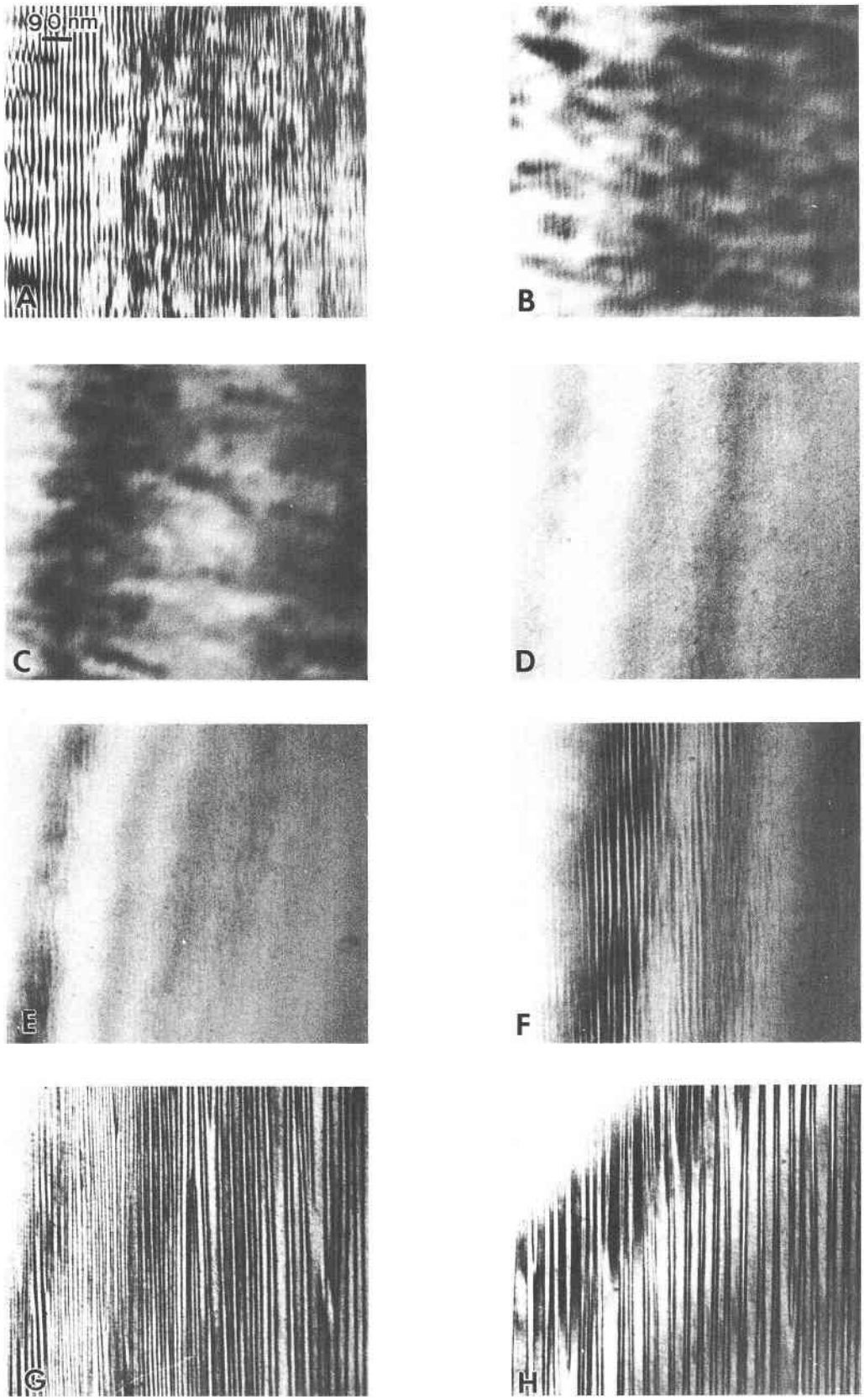
90 nm
A
B
C
D
E
F
G
H

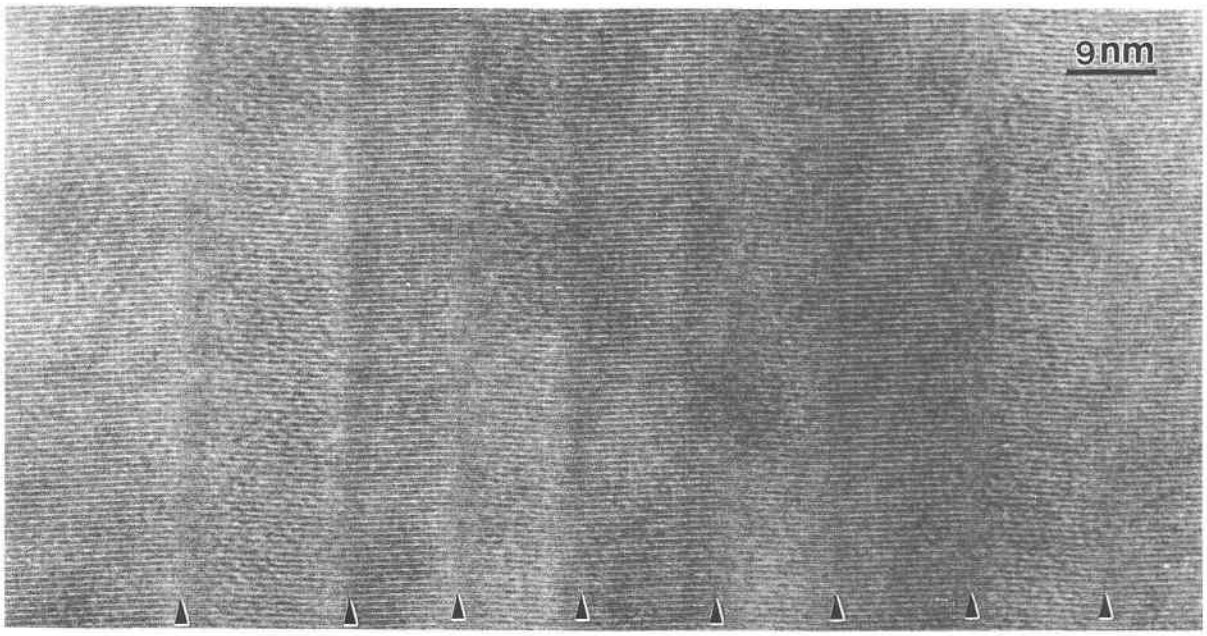

Fig. 10. HRTEM image of Na-rich feldspar following a heating and cooling cycle shows relatively finer and coarser triclinic layer domains in the albite-twin relationship (arrows indicate twin boundaries). In contrast to the unheated sample, the (001) lattice fringes are chevronlike. Best viewed at a low angle parallel to the fringes.

weakly first-order transition in character. The narrower, critical temperature range observed in the second heating and cooling cycle may be due to compositional homogenization of the previously heated specimen. The phase transitions from modulated and triclinic ($C\bar{1}$) structures to the monoclinic structure ($C2/m$) are quite rapid, which further indicates displacive transitions according to Buerger's classification for structural phase transitions (Buerger, 1972). Therefore, the modulation in the feldspar probably results from, or is at least dominated by, atomic displacements from the ideal monoclinic atomic positions rather than Si-Al ordering or a K-Na compositional modulation.

Interpretation of the TEM results

A proposed displacive phase-transition line for alkali feldspar containing 5% anorthite component is illustrated in Figure 11, along with the coherent spinodal that applies to exsolution in alkali feldspar. The displacive phase-transition boundary is drawn on the basis of Kroll and Bambauer's data (Kroll and Bambauer, 1971) and our heating and cooling results. The phase-transition temperature for our Na-rich feldspar sample is lower than the coherent spinodal. However, spinodal decomposition did not occur in the Na-rich feldspar, probably because of extremely fast cooling of the crystal, except perhaps in limited areas that show very weak contrast that could result from compositional variations (e.g., Fig. 3B).

As noted above, the modulated structure characterized by wavelike (001) lattice fringes can be considered as a periodic arrangement of triclinic (010) layer domains in the albite-twin relationship. It is probably an intermediate but not a thermodynamically stable structure between equilibrium feldspars with monoclinic ($C2/m$) and triclinic ($C\bar{1}$) symmetry. A Na-rich feldspar with this kind of structural modulation may be characteristic of feldspars that have undergone very rapid cooling from high temperatures. Line A-B in Figure 11 shows the cooling path of the Na-rich feldspar. The modulated structure presumably was formed below the temperature of the displacive phase transition from $C2/m$ to $C\bar{1}$ symmetry.

A MODEL FOR THE FORMATION OF THE MODULATED STRUCTURE

On the basis of TEM results and the heating and cooling experiments on the feldspar crystal, it appears that the modulated structure arises only when the phase transition from the monoclinic ($C2/m$) to the triclinic ($C\bar{1}$) structure is inhibited. No modulated structure forms in the crystal during the reverse transition, from triclinic to monoclinic structure. Therefore, there is no evidence of a stability field for the modulated structure of Na-rich alkali feldspar; by contrast, the modulated structures in intermediate plagioclase appear to have a true stability field (Carpenter, 1986). The modulated structure in the Na-rich alkali feldspar instead should be treated as a non-

←

Fig. 9. BF images of Na-rich feldspar during heating and cooling. (**A**) 366 °C (heating), (**B**) 535 °C (heating), (**C**) 702 °C (heating), (**D**) 840 °C (heating), (**E**) 440 °C (cooling), (**F**) 300 °C (cooling), and (**G** and **H**) 25 °C (cooling). All images are at same magnification.

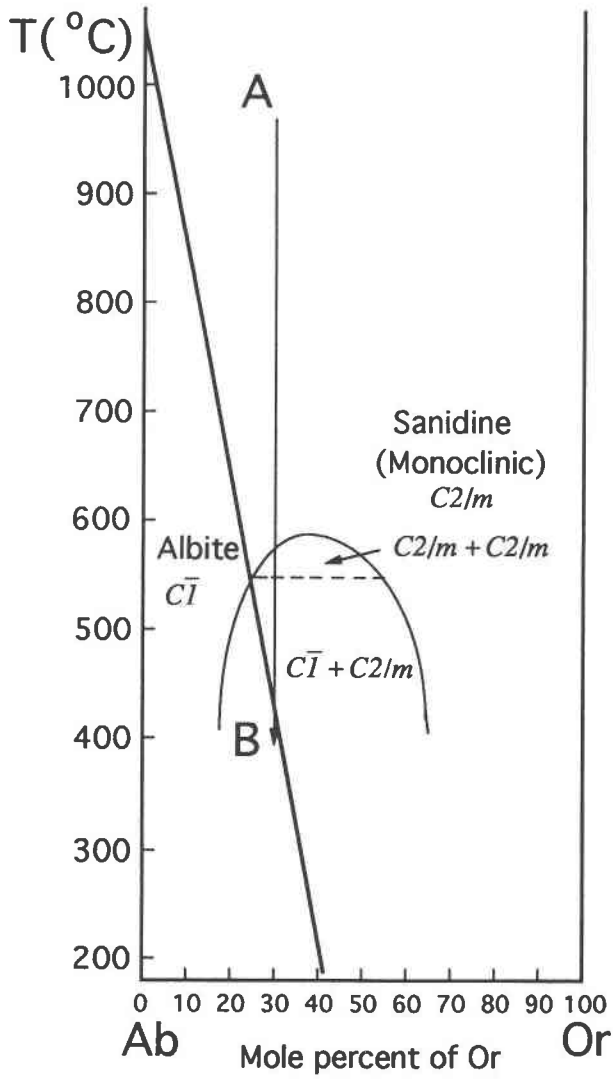

Fig. 11. A possible phase diagram for alkali feldspars (modified from Smith and Brown, 1988; Yund, 1983, 1984; Kroll and Bambauer, 1971). The straight phase-transition line for alkali feldspars with 5% anorthite component is drawn on the basis of Kroll and Bambauer's (1971) data and the in situ experiment of this study. The modulated structure in our sample probably formed during the displacive phase transition from $C2/m$ to $C\bar{1}$ symmetry as the Na-rich feldspar crystal cooled from A to B at a relatively fast rate.

equilibrium phase resulting from kinetic phenomena. Here we develop a heuristic model for the mechanism causing the periodic atomic-displacement modulation in Na-rich feldspar.

The heating experiments described above are consistent with a displacive phase-transition in Na-rich feldspar that is a weak first-order phase transition. As a first approximation, the potential (G) for the Na-rich feldspar below the equilibrium phase-transition temperature (T_c) may be expressed as the Landau potential for a second-order phase transition,

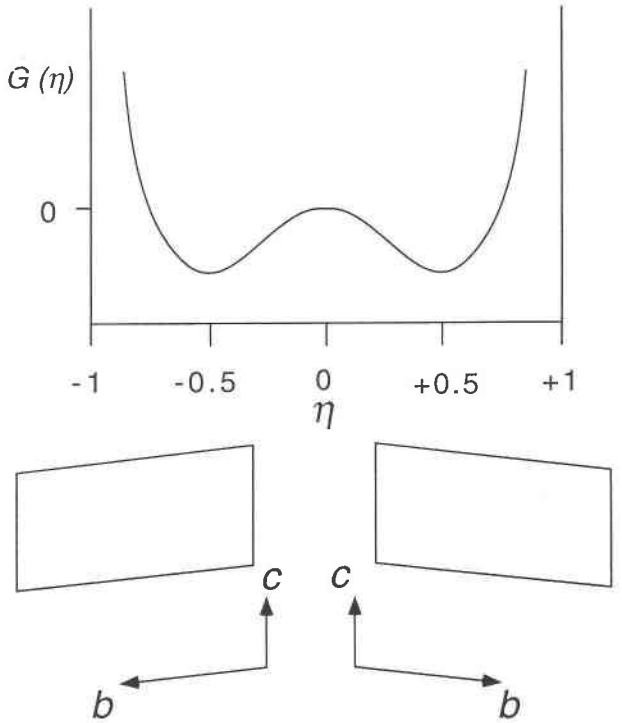

Fig. 12. Potential $G(\eta)$ of the Na-rich feldspar at $T < T_c$. The two potential wells are low-energy states for the triclinic feldspar structure. Positive and negative order parameters correspond to two different orientations of the triclinic structures that are in the albite-twin relationship.

$$G(\eta) = \beta\left(\frac{B}{4}\eta^4 - \frac{A}{2}\eta^2\right) \quad (1)$$

where η is an order parameter indicating the degree of structural deviation from monoclinic symmetry below T_c (Landau and Lifshitz, 1969). The parameters A, B, and β are dependent on temperature and composition. The potential is changed by adjusting the parameters in Equation 1. The equilibrium order parameter (η_{equi}) for the crystal at temperature $T < T_c$ is

$$\eta_{equi} = \pm\sqrt{\frac{A}{B}}. \quad (2)$$

As an example, the potential for parameters $A = 1$, $B = 4$, $\beta = 0.5$, and $\eta = \pm 0.5$ is plotted in Figure 12. In the absence of a stress field, the probabilities for triclinic structures with $\eta = +0.5$ and $\eta = -0.5$ are the same. Physically, the positive and negative order parameters for the lower-symmetry phase represent the two different orientations of the triclinic structure that are related by the albite-twin relationship. Therefore, the triclinic structure formed by transformation from the monoclinic structure can occur with two different distortions having positive and negative order parameters, respectively.

On the basis of the potential at $T < T_c$, we obtain a driving force for the phase transition from the high-temperature (high-symmetry) structure to the low-temperature (low-symmetry) structure. Taking Equation 1 as the

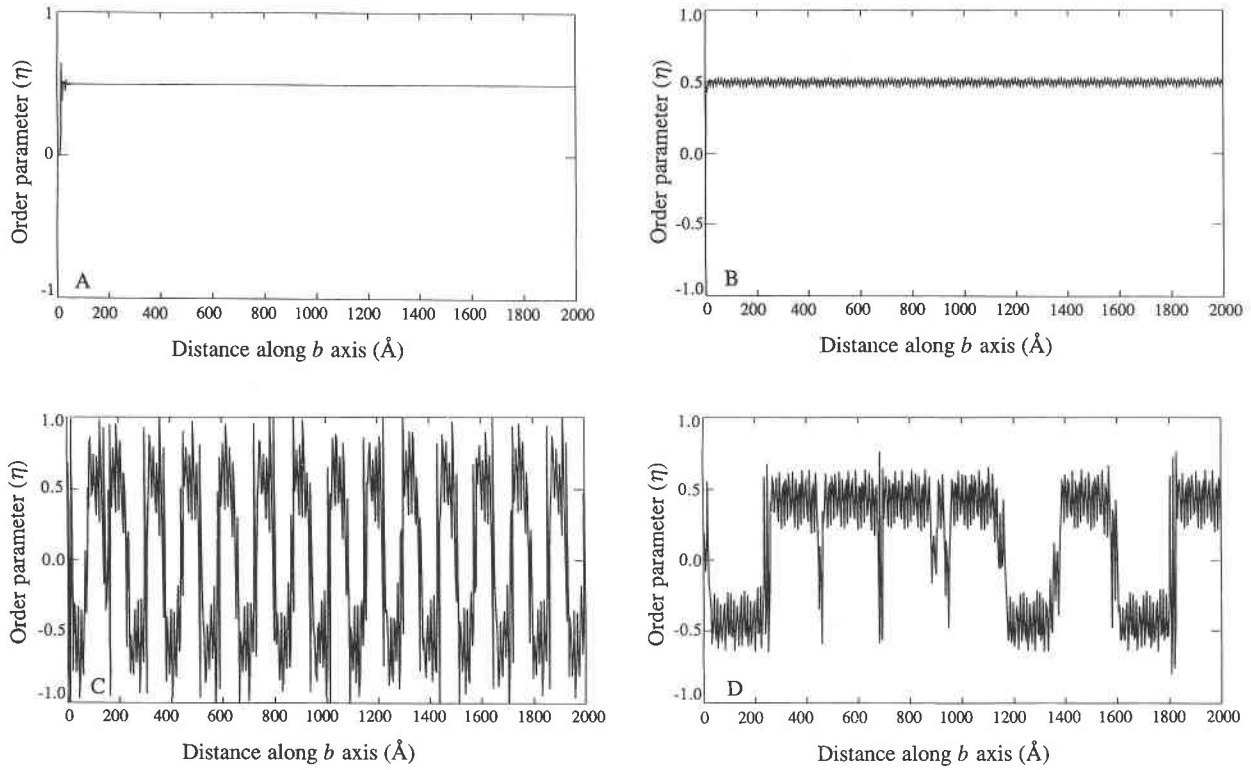

Fig. 13. Some numerical solutions of Eq. 7. **A** is at the equilibrium state ($\gamma = 0$). **B** is near the equilibrium state ($\gamma = 0.1$, $\sigma = 0.4$, $\beta = 2$, $A = 1$, $B = 4$). **C** is at a nonequilibrium state exhibiting periodic oscillation of the order parameter ($\gamma = 0.3$, $\sigma = 0.34$, $\beta = 1$, $A = 1$, $B = 2$), and **D** is at a nonequilibrium state showing nonperiodic oscillation of the order parameter ($\gamma = 0.4$, $\sigma = 0.415$, $\beta = 1.96$, $A = 1$, $B = 4$). **C** and **D** correspond to periodic and nonperiodic arrangements of triclinic albite-twin domains.

potential for the Na-rich feldspar, the driving force for the phase transition is

$$-\nabla G(\eta) = \ddot{\eta} \tag{3}$$

or

$$\nabla G(\eta) + \ddot{\eta} = 0 \tag{4}$$

where

$$\nabla G(\eta) = \beta(B\eta^3 + A\eta). \tag{5}$$

In the above equations, $\ddot{\eta}$ is the rate of change of $\dot{\eta}$, whereas $\dot{\eta}$ is the rate of change of the order parameter. The force represented by Equation 5 drives the monoclinic structure (i.e., $\eta = 0$) to a triclinic structure with lower energy at $T < T_c$. The additional force (or stress) induced by structural differences between neighboring unit cells with different order parameters is proposed to be proportional to the rate of change of the order parameter ($\dot{\eta}$) or the rate of structural variation (i.e., a damping term $\sigma\dot{\eta}$). Adding the damping term $\sigma\dot{\eta}$ to Equation 4 gives

$$\nabla G(\eta) + \ddot{\eta} + \sigma\dot{\eta} = 0. \tag{6}$$

This equation describes a damped structural oscillation at $T < T_c$ without an external force.

For the nonequilibrium phase transition, an external force acting on the feldspar crystal may be introduced. By simply assuming that the external force affecting the distortion of the monoclinic lattice to the triclinic lattice is periodic, and that it possesses the same periodicity as the Na-rich feldspar crystal along the **b** axis, we write the external force as $F = \gamma \cos(\omega b)$. Here $\omega = 2\pi/b_0$ ($b_0 \cong 13$ Å), and $\gamma = 0$ only at the equilibrium state.

Adding the external force to Equation 6 gives

$$\nabla G(\eta) + \ddot{\eta} + \sigma\dot{\eta} = \gamma \cos(\omega b). \tag{7}$$

This equation describes a damped structural oscillation at $T < T_c$ with an external force due to the nonequilibrium condition. Equation 7 is similar to Duffin's equation that describes forced oscillations (Guckenheimer and Holmes, 1983; Thompson and Stewart, 1986). The equation can be solved numerically.

In general, the solutions to Equation 7 are nonperiodic, and they are very sensitive to all adjustable parameters. Only at the equilibrium condition (i.e., $\gamma = 0$ for the equilibrium phase transition) or near equilibrium ($\gamma \cong 0$) is the transformed phase a homogeneous, untwinned triclinic crystal with either positive or negative order parameter (Fig. 13A and 13B). A schematic diagram of such an untwinned crystal is shown in Figure 14A. Under special conditions (for instance, fast cooling), the order parameter behaves periodically, resulting in a periodic arrangement of triclinic domains with two different orientations along the **b** axis) (Figs. 13C and 14B). Ac-

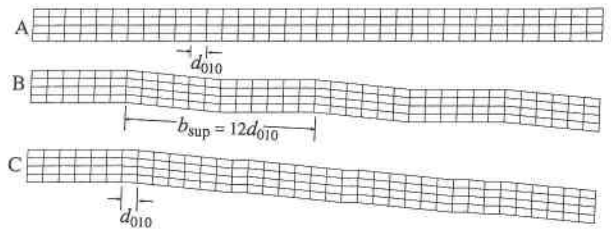

Fig. 14. Schematic diagrams showing arrangements of triclinic domains at different conditions. (A) Homogeneous triclinic structure corresponding to the solutions of Fig. 13A and 13B. (B) Periodic arrangement of triclinic domains corresponding to the solution of Fig. 13C. (C) Nonperiodic arrangement of triclinic domains corresponding to the solution of Fig. 13D.

tually, these arrangements are quasiperiodic rather than truly periodic because the details of amplitude and periodicity are not the same for every oscillation. This is seen by examining the detailed oscillations of the peaks and valleys in Figure 13C. Such structural oscillation in Na-rich feldspar would cause satellite reflections in diffraction patterns, as observed with SAED. We suggest that the periodic modulation in the feldspar sample with average periodicity of $14d_{010}$ ($\cong$180 Å) may be such a one-dimensional structural oscillation that arose during the phase transition from $C2/m$ symmetry to $C\bar{1}$ symmetry. One example of a numerical solution with a nonperiodic structural oscillation is illustrated in Figure 13D. The arrangement of triclinic domains along the **b** axis corresponding to Figure 13D is illustrated schematically in Figure 14C. Such nonperiodic twinning is common in natural Na-rich alkali feldspars.

Thus, according to the proposed model, the triclinic domains formed at the $C2/m$ to $C\bar{1}$ transition of Na-rich feldspar generally are nonperiodic. Periodic arrangements of triclinic domains along the **b** axis (i.e., periodic, one-dimensional structural modulations) form only under special conditions (e.g., certain cooling rates) that are relatively far from the equilibrium state. Only after we know the relationship among the damping coefficient, external force, temperature, and cooling rate is it possible to predict the conditions for formation of the modulated structures. Also, according to this model, the modulated Na-rich feldspar is not a thermodynamically stable phase. There is no field of stability for the modulated structures, nor do they arise as metastable phases because they have lower energies than nonperiodically twinned Na-rich feldspar. This is in contrast to the modulated structures of intermediate plagioclase, which were revealed by Carpenter (1986) to represent relatively stable states.

Acknowledgments

We thank Gufeng Luo of Nanjing University and John Ferry of Johns Hopkins University for helpful discussion, and Michael A. Carpenter of Cambridge University for critical review and helpful comments. This work was supported by NSF grant EAR-8903630, and electron microscopy was performed in the HRTEM laboratory at Johns Hopkins University, which was established with partial support from NSF grant EAR-8300360.

References cited

Buerger, M.J. (1972) Phase transformations. Soviet Physics—Crystallography, 16, 959–968.

Carpenter, M.A. (1986) Experimental delineation of the "e" = $I\bar{1}$ and "e" = $C\bar{1}$ transformations in intermediate plagioclase feldspars. Physics and Chemistry of Minerals, 13, 119–139.

Deer, W.A., Howie, R.A., and Zussman, J. (1965) Rock-forming minerals, vol. 4, p. 1–93. Wiley, New York.

Guckenheimer, J., and Holmes, P. (1983) Nonlinear oscillations, dynamical systems, and bifurcations of vector fields, 453 p. Springer-Verlag, New York.

Kroll, H., and Bambauer, H.-U. (1971) The displacive transformation of (K,Na,Ca)-feldspars. Neues Jahrbuch für Mineralogie Monatshefte, 413–416.

Kroll, H., Bambauer, H.-U., and Schirmer, U. (1980) The high albite-monalbite and analbite-monalbite transitions. American Mineralogist, 65, 1192–1211.

Landau, L.D., and Lifshitz, E.M. (1969) Statistical physics, 484 p. Pergamon, Oxford, U.K.

Laves, F. (1950) The lattice and twinning of microcline and other potash feldspars. Journal of Geology, 58, 548–571.

——— (1960) The feldspars, their polysynthetic twinning and their phase relations. Rendiconti della Società Italiana di Mineralogia e Petrologia, 16, 37–100.

McConnell, J.D.C. (1971) Electron optical study of phase transformation. Mineralogical Magazine, 38, 1–20.

Owen, D.C., and McConnell, J.D.C. (1974) Spinodal unmixing in an alkali feldspar. In W.S. MacKenzie and J. Zussman, Eds., The feldspars, p. 424–439. Manchester University Press, Manchester, U.K.

Ribbe, P.H. (1983) Aluminum-silicon order in feldspars: Domain textures and diffraction patterns. In Mineralogical Society of America Reviews in Mineralogy, 2, 21–55.

Smith, J.V., and Brown, W.L. (1988) Feldspar minerals, vol. 1, p. 1–20, 541–542. Springer-Verlag, Berlin.

Smith, K.L., McLaren, A.C., and O'Donnell, R.G. (1987) Optical and electron microscope investigation of temperature-dependent microstructures in anorthoclase. Canadian Journal of Earth Science, 24, 528–543.

Thompson, J.M.T., and Stewart, H.B. (1986) Nonlinear dynamics and chaos: Geometrical methods for engineers and scientists, 376 p. Wiley, Chichester, U.K.

Veblen, D.R. (1985) Direct TEM imaging of complex structures and defects in silicates. Annual Review of Earth and Planetary Sciences, 13, 119–146.

Winchell, A.N., and Winchell, H. (1967) Elements of optical mineralogy: II. Descriptions of minerals, p. 311. Wiley, New York.

Xu, H. (1993) Transmission electron microscopy study of nonperiodic structures in silicate minerals. Ph.D. dissertation, Johns Hopkins University, Baltimore, Maryland.

Xu, H., and Veblen, D.R. (1993) Structural modulation and phase transition in anorthoclase: Transmission electron microscopy study (abs.). Feldspars and Their Reactions, Programme and Abstracts of the NATO Advanced Study Institute, p. 13. Edinburgh, Scotland.

Xu, H., Veblen, D.R., and Luo, G. (1995) A new commensurate modulated structure in orthoclase. Acta Crystallographica, A51, 53–60.

Yund, R.A. (1983) Kinetics and mechanisms of alkali feldspar exsolution. In Mineralogical Society of America Reviews in Mineralogy, 2, 177–202.

——— (1984) Alkali feldspar exsolution: Kinetics and dependence of alkali interdiffusion. In W.L. Brown, Ed., Feldspars and feldspathoids, p. 281–315. Reidel, Dordrecht, the Netherlands.

Zhou, X., and Chen, T. (1982) Study of the megacryst inclusions in the Cenozoic alkali basalt of the Eastern Coast of China. Acta Mineralogica Sinica, 2, 13.

Manuscript received June 6, 1994
Manuscript accepted May 31, 1995